

1       **The climates of Earth's next supercontinent: effects of**  
2               **tectonics, rotation rate, and insolation**

3               **M. J. Way<sup>1,2,3</sup>, H. S. Davies<sup>4,5</sup>, J. C. Duarte<sup>4,5,6</sup>, and J. A. M. Green<sup>7</sup>**

4                               <sup>1</sup>NASA Goddard Institute for Space Studies, New York, USA

5                               <sup>2</sup>Goddard Space Flight Center Sellers Exoplanet Environments Collaboration

6                               <sup>3</sup>Theoretical Astrophysics, Department of Physics and Astronomy, Uppsala University, Uppsala, Sweden

7                               <sup>4</sup>Instituto Dom Luiz (IDL), Faculdade de Ciências, Universidade de Lisboa, Lisbon, Portugal

8                               <sup>5</sup>Departamento de Geologia, Faculdade de Ciências, Universidade de Lisboa, Lisbon, Portugal

9                               <sup>6</sup>School of Earth, Atmosphere and Environment, Monash University, Melbourne, Victoria, Australia

10                               <sup>7</sup>School of Ocean Sciences, Bangor University, Menai Bridge, UK

11       **Key Points:**

- 12       • The climate of a distant future Earth is modeled for two different supercontinent  
13       scenarios.
- 14       • The latitudinal location of the supercontinents are critical to mean surface tem-  
15       peratures.

---

Corresponding author: Michael Way, [michael.way@nasa.gov](mailto:michael.way@nasa.gov)

## Abstract

We explore two possible Earth climate scenarios, 200 and 250 million years into the future, using knowledge of the evolution of plate tectonics, solar luminosity, and rotation rate. In one scenario, a supercontinent forms at low latitudes, whereas in the other it forms at high northerly latitudes with an antarctic subcontinent remaining at the south pole. The climates between these two end points are quite stark, with differences in mean surface temperatures approaching 4 degrees. The fractional habitability (mean surface temperatures remaining between  $0 < T < 100^\circ$  year round) on land is shown to differ as much as 40% between the two simulations. These results demonstrate the need to consider alternative boundary conditions when simulating Earth-like exoplanetary climates.

## Plain Language Summary

We investigate two tantalizing Earth climate scenarios 200 and 250 million years into the future. We show the role played by plate tectonics, the sun's increase in brightness, and a slightly slower rotation rate in these future climate scenarios. In one case the present day continents form into a single land-mass near the equator, and in the other case Antarctica stays put, but the rest of the present day continents are mostly pushed well north of the equator. The difference in the mean surface temperatures of these two cases differ up to 4 degree Celsius, while also being distinct in the total surface area in which they maintain temperatures allowing liquid water to exist year round.

## 1 Introduction

Earth's near-future climate has been extensively explored via the IPCC and associated CMIP studies (e.g. Collins et al., 2013). Earth's ancient climate has also been studied at various levels of detail, including the Cretaceous greenhouse (e.g., Huber et al., 2018), the Neoproterozoic Snowball (Pierrehumbert et al., 2011), and on the supercontinent Pangea (e.g., Parrish, 1993). Earth's deep time future is a novel research discipline, and changes in deep-time future climate, induced by changes in topography and land/sea masks (e.g., Davies et al., 2018), have yet to be explored until now.

The geological formations on the ever-changing surface of the Earth have a strong influence on our climate. The separation of Australia from Antarctica (DeConto & Pollard, 2003) and the opening of the Drake Passage (Barker, 2001) 30–40 million years ago induced the Antarctic glaciation. The development of the Caribbean arc and closing of the Panama Isthmus allowed the Gulf Stream to form, with major consequences for global climate (Montes et al., 2015). A closure of the Strait of Gibraltar led to the Messinian Salinity Crisis (Krijgsman et al., 1999), whereas the Himalayas, a consequence of the India-Eurasia collision, allows for the monsoon (Tada et al., 2016). Recently, Farnsworth et al. (2019) showed that the climate sensitivity for the period 150–35 million years ago is dependent on the continental configuration, particularly ocean area. Schmittner et al. (2011) investigated the effects of mountains on ocean circulation patterns of present day Earth and concluded that the current configuration of mountains and ice sheets determines the relative deep-water formation rates between the Atlantic and the Pacific Oceans.

The tectonic plates on Earth aggregate into supercontinents and then disperse on a cycle of 400-600 million years – the supercontinent cycle (Davies et al., 2018; Pastor-Galán et al., 2019; Yoshida, 2016; Yoshida & Santosh, 2018). The latest supercontinent, Pangea, formed around 310 million years ago, and started breaking up around 180 million years ago. The next supercontinent will most likely form in 200–250 million years, meaning Earth is currently about halfway through the scattered phase of the current supercontinent cycle (Davies et al., 2018).

63 There are obvious and strong links between large scale tectonics and climate. It  
64 would be interesting to know what Earth's climate could be like in the distant future,  
65 when continental movements have taken Earth away from the current continental con-  
66 figuration (Davies et al., 2018). This will be explored here, where we investigate what  
67 the climate may look like on Earth in a future supercontinent state. A secondary appli-  
68 cation of climate modelling of the deep-time future is to create a climate model of an Earth-  
69 like exoplanet using the parameters known to sustain habitability and a stable biosphere  
70 (Earth). Using the Deep-time future Earth as a basis for exoplanetary climate studies  
71 allows us to establish sensitivity ranges for the habitability and climate stability of the  
72 future Earth and its distant cousins in our Milky Way Galaxy.

## 73 2 Methods

### 74 2.1 Tectonic maps

75 Maps of the future Earth were produced based on two plausible scenarios for fu-  
76 ture Earth: Aurica (forming around 250 million years from now; see Duarte et al., 2018)  
77 and Amasia (forming around 200 million years from now; Mitchell et al., 2012) – see  
78 Davies et al. (2018) for a summary. In both cases the ocean bathymetry was kept as in  
79 Davies et al. (2019), with continental shelf seas 150 m deep, mid-ocean ridges 1600 m  
80 deep at the crest point and deepening to the abyssal plains within  $5^\circ$ , and subduction  
81 zones 6000 m deep. The abyssal plain was set to a depth maintaining the present day  
82 ocean volume. Each topographic file was generated with a  $1/4^\circ$  horizontal resolution in  
83 both latitude and longitude.

84 We generated three subsets of maps for each of the two supercontinent scenarios  
85 (see Table 1):

- 86 1. Low mean topography (land close to sea level), with no mountains (CTRL)
- 87 2. Higher mean topography (land close to present day mean topography) with no moun-  
88 tains (PD)
- 89 3. Low topography with mountains (land close to sea level interspersed with moun-  
90 tains) (MTNS)

91 The first subset of maps serve as a control (CTRL), allowing us to test the effect of the  
92 position and geometry of the continents without the influence of high topographies and  
93 particular features such as mountain ranges. It could also simulate a supercontinent that  
94 has existed long enough to have been almost fully eroded. The land here has been as-  
95 signed topography with a normal distribution (mean = 1 m and standard deviation =  
96 50 m), giving topographic heights varying from 1 to 200 m.

97 The second set of maps assume mean topographic values close to those of present  
98 day (PD) but with no significant variation (e.g., no high mountains). This was made by  
99 applying a random topography following a normal distribution with mean and standard  
100 deviations closer to those of present day Earth's topography (i.e., mean of 612 m and  
101 standard deviation of 712 m). The resulting topography varies between 1 and 4000 m  
102 in height.

103 In the third set (MTNS), we included mountain ranges. The land of the supercon-  
104 tinent was first given a random topography similar to the control map (varying randomly  
105 between 1 and 200 m), after which mountains were added manually. The mountains are  
106 of three types: 1) Himalaya-type, which result from the collision of continents during the  
107 formation of the supercontinent, with an average peak elevation of 7500 m; 2) Andes-  
108 type, located at the margins of the continents along major subduction zones, with an  
109 average peak elevation of 4000 m; and 3) Appalachian-type, which correspond to eroded  
110 orogens that were formed and then partially eroded during the supercontinent cycle, with

**Table 1.** A summary list of the simulations & results.

Sim	Name	Topography	I <sup>a</sup>	LoD <sup>b</sup>	Runtime (years)	T <sup>c</sup> (C)	Balance (Wm <sup>-2</sup> )	A <sup>d</sup> (%)	SnowFr <sup>e</sup> (%)
Aurica									
01	Aurica_Rand_CTRL	CTRL	1.0260	24.5	2000	20.5	0.23	30.5	0.5
02	Aurica_Rand_PD	PD	"	24.5	2500	20.6	0.10	30.1	0.6
03	Aurica_250f	MTNS	"	24.5	2000	20.6	0.20	30.3	1.5
Amasia									
04	Amasia_Rand_CTRL	CTRL	1.0223	24.5	2567	19.7	0.42	30.1	4.2
05	Amasia_Rand_PD	PD	"	24.5	3000	17.2	0.25	31.1	9.0
06	Amasia_200f	MTNS	"	24.5	3000	20.2	0.24	30.0	4.7
Earth									
07	Earth_noAer_noO3	-	1.0	24.0	1000	14.2	0.17	31.1	11.1

<sup>a</sup> Insolation, where 1.0 = 1361 W m<sup>-2</sup> (Modern Earth).

<sup>b</sup> LoD = Length of Day in hours.

<sup>c</sup> Global mean surface temperature in degrees Celsius from an average over the last 10 years of the model run.

<sup>d</sup> Planetary Albedo.

<sup>e</sup> Snow and Ice, global fractional area.

111 an average peak elevation of 2000 m. In all cases, the width of the mountains is 5° from  
112 peak to base.

## 113 2.2 Rotation changes

114 Day-length for the future was computed based on the simulated tidal dissipation  
115 rates presented in Green et al. (2018). The tidal dissipation rates at the supercontinent  
116 state is only about 20% of that at present, leading to a change in day length that can-  
117 not be ignored. The time rate of change in Earth’s angular rotation rate,  $d\Omega/dt$ , can be  
118 approximated by (MacDonald, 1964)

$$\frac{d\Omega}{dt} = \frac{45}{8} k \frac{Gm^2 A^3}{Mr^6} \sin(2\alpha) \quad (1)$$

119 Here  $k = 0.2$  is a Love number,  $G = 6.67 \times 10^{-11} \text{ m}^3 \text{ kg}^{-1} \text{ s}^{-2}$  is the gravitational  
120 constant,  $m = 7.3 \times 10^{22} \text{ kg}$  is the moon’s mass,  $M = 6 \times 10^{24} \text{ kg}$  is the Earth’s mass,  
121  $A = 6.4 \times 10^6 \text{ m}$  is Earth’s mean radius,  $r = 3.8 \times 10^8 \text{ m}$  is the Earth-moon distance,  
122 and is the angle ( $\alpha$ ) between the tidal bulge and the Earth-moon center line. The lat-  
123 ter is defined from  $\sin(2\alpha) = D/W$ , i.e., the ratio between the tidal dissipation rate  $D$   
124 and the work done by the tide generating force,  $W$ ; both are computed by the numer-  
125 ical tidal model used in Green et al. (2018).

126 The resulting spin down is  $d\Omega/dt = 2.23 \times 10^{-22} \text{ s}^{-2}$ , or the equivalent of a length-  
127 ening of a day by 0.5 hours over 200 million years (My). This length of day (24.5 hours)  
128 was consequently used in the General Circulation Model simulations discussed below.

## 129 2.3 General Circulation Model set up

130 The ROCKE-3D General Circulation Model (GCM) version Planet\_1.0 (R3D1) as  
131 described in Way et al. (2017) is utilized for this study. A fully coupled dynamic ocean  
132 is utilized. Data from Claire et al. (2012) (see their Table 2) is used to estimate the so-  
133 lar flux  $\sim 250 \text{ My}$  into the future impinging upon Earth. We do not change the solar spec-  
134 trum as the changes for such a small leap into the future will be minimal in terms of its  
135 effect on Earth’s atmosphere. We use an insolation value of 1.019 estimated as the mean  
136 of today’s value of 1 and the value 500 My into the future of 1.037 from Claire et al. (2012).  
137 Hence the insolation in  $\text{W m}^{-2}$  is  $1361 \times 1.019 = 1397 \text{ W/m}^{-2}$ .

138 We use a 50/50 clay/sand mix for the soil given that we have no constraints on what  
 139 the surface will be like in the deep future and is a value commonly used in the exoplanet  
 140 community (e.g. Yang et al., 2014; Way et al., 2018). 40 cm of water is initially distributed  
 141 into each soil grid cell. We use a ground albedo of 0.2 at model start, but the albedo will  
 142 change via snow deposition (brighter), or from rainfall (darker) as the GCM moves for-  
 143 ward in time.

144 The original topography resolution of  $1/4^\circ \times 1/4^\circ$  from the tectonic maps discussed  
 145 in Section 2.1 is down-sampled to a resolution of  $4^\circ \times 5^\circ$  in latitude by longitude, which  
 146 is the default R3D1 resolution. The standard deviation from the down-sampling is used  
 147 to set the roughness length of the surface in each grid cell. River flow direction is based  
 148 on the resulting topography and exits to the ocean when possible. Large inland seas (typ-  
 149 ically less than 15 contiguous grid cells) are defined as lakes rather than ocean grid cells.  
 150 The GCM allows lakes to expand and contract as dictated by the competition between  
 151 evaporation and precipitation. The same holds for the possible creation and disappear-  
 152 ance of lakes. This allows the model to handle inland surface water in a more sophisti-  
 153 cated manner than making all surface water defined as ocean grid cells. This is highly  
 154 desirable because ocean grid cells cannot be created or destroyed during a model run.

155 Any ocean grid cell with a depth less than 150 meters (from the down-sampled  $4^\circ \times$   
 156  $5^\circ$  data) was set to have a value of 204 meters (the mean depth of ocean model level 6).  
 157 This is especially important at high latitudes where the ocean may freeze to the bottom,  
 158 which will cause the model to crash due to its inability to dynamically change surface  
 159 types from ocean to land ice.

160 The down-sampling has a side effect in that the land-sea mask will differ slightly  
 161 between the three topographic types (CTRL, PD, MTNS). For example, in a case with  
 162 a collection of ocean or lake grid cells adjacent to a number of high elevation land to-  
 163 pography grid cells the down-sampling may change the combined ocean + land grid cells  
 164 into a land grid cell, or vice-versa if the mean of the ocean grid cells is larger than that  
 165 of the land grid cells. This is why the land/sea masks differ between CTRL, PD and MTNS  
 166 in Figure 1, even though their  $1/4^\circ \times 1/4^\circ$  parents had exactly the same land-sea mask.

167 The atmosphere is set to roughly Earth constituents in the year 1850: Nitrogen dom-  
 168 inated with 21% Oxygen, 285 ppmv  $\text{CO}_2$ , 0.3 ppmv  $\text{N}_2\text{O}$ , and 0.79 ppmv  $\text{CH}_4$ . No aerosols  
 169 or Ozone ( $\text{O}_3$ ) are included. For comparison purposes we include a modern Earth-like  
 170 land/sea mask (Simulation 07: Earth\_noAer\_noO3) with these same atmospheric con-  
 171 stituents, but with modern insolation ( $1361 \text{ W m}^{-2}$ ) and a bathtub ocean. The Earth-  
 172 like land/sea mask is described in Way et al. (2018) and shown in Figure 8 of that pa-  
 173 per.

### 174 3 Results

175 Previous work has shown that ancient Earth supercontinent phases, which are com-  
 176 parable to our Aurica Simulations 01-03, have had more arid interiors where weather-  
 177 ing effects and  $\text{CO}_2$  draw down may have been less efficient (e.g. Jellinek et al., 2019).  
 178 This would increase surface temperatures as the balance of  $\text{CO}_2$  would tend to be larger  
 179 than present day because volcanic outgassing (sources) would likely remain constant while  
 180  $\text{CO}_2$  drawdown (sinks) would decrease. However, there are other climatic effects to con-  
 181 sider. For example, the Amasia reconstruction is essentially an arctic supercontinent with  
 182 an independent and isolated antarctic continent, meaning both poles are covered by land,  
 183 and much of that is covered by ice. Amasia is thus in essence a shift to consolidate the  
 184 present day domination of northern latitude land masses even further north.

185 This increase in land masses at northerly latitudes means that there is less ocean  
 186 heat transport to melt the ice in the northern hemisphere summers. Consequently, more  
 187 ice resides on land and in lakes all year round near the north pole, as we see in present

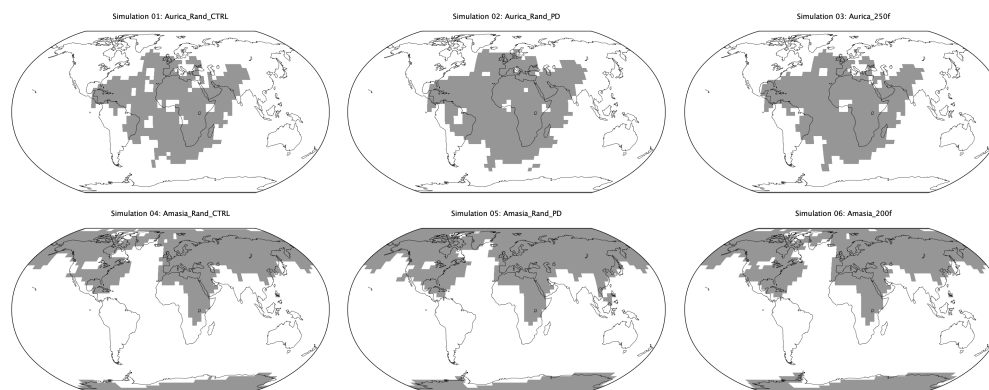


**Figure 1.** Land (grey) and Sea (white) masks used in experiments of Table 2.1. Present day Earth continental outlines are shown for reference.

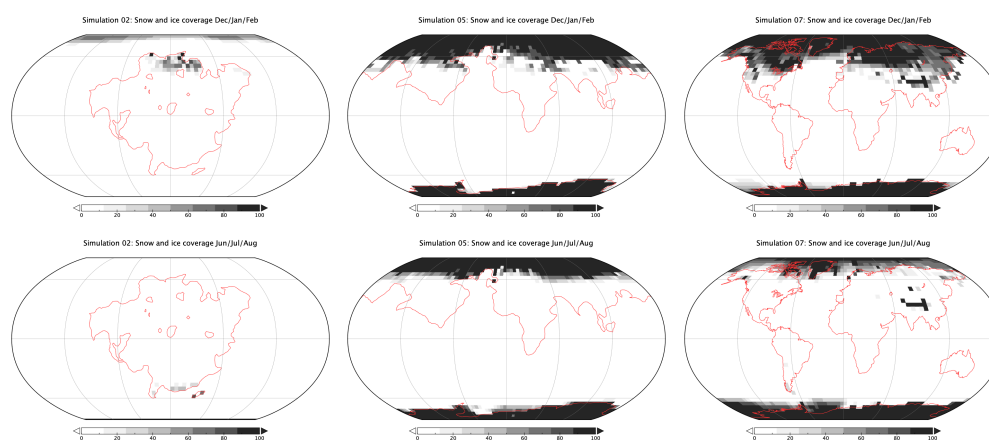


**Figure 2.** Individual grid cell snow+ice fractional amounts. For Simulation 02 (left), Simulation 05 (middle) and Simulation 07 (right) for a sum of the months of December, January and February (top) and June, July and August (bottom) in the last year of each simulation.

188 day Antarctica. This is the well known ice-albedo climate feedback and explains why these  
 189 simulations tend to be cooler than the others. The coolest simulation is Simulation 05  
 190 (Amasia\_Rand\_PD), because it has very very few inland seas in the north (compared to  
 191 Simulations 04 & 06) that could thaw out in the summers, as well as less ocean area at  
 192 high latitudes to transport heat. Hence, it tends to remain cooler than Simulations 04  
 193 & 06 with similar land/sea masks (see Figure 1).

194 It is informative to contrast Simulation 02 (Aurica\_Rand\_PD) with Simulation 05  
 195 (Amasia\_Rand\_PD). Simulation 02 is more contiguous (less inland lakes & seas), has land  
 196 at lower latitudes and uses the same “present day” (PD) topographic values for inputs  
 197 as Simulation 05. Simulation 05 also has contiguous land, but at much higher latitudes.  
 198 In Table 2.1 we give their mean surface temperatures, planetary albedo and fractional  
 199 snow & ice coverage. The snow & ice coverage in particular is clearly the biggest climatic  
 200 factor as shown in Figure 2. There, we show the seasonal snow & ice coverage for Sim-  
 201 ulations 02 & 05 where Dec/Jan/Feb is an average over northern hemisphere winter months  
 202 December, January & February. Jun/Jul/Aug is an average over the northern hemisphere  
 203 summer months of June, July & August. We could have used albedo, but it is an im-  
 204 perfect measure here since in the northern winter months much of the area above the

205 Arctic circle gives null values (no reflected light, hence no albedo) and the same during  
206 the southern winter months for land areas below the Antarctic circle. Regardless, in Ta-  
207 ble 2.1 it is clear that the snow & ice fractions are much higher for the Amasia runs (04,  
208 05, 06) compared to the other three Aurica runs (01, 02, 03), and highest for Simulation  
209 05 in particular. The higher snow fraction amount of Simulation 05 corresponds directly  
210 to the lower surface temperature in this set of runs. This coldest of the future climates  
211 (Simulation 05) has a similar global 10 year mean albedo to that of Simulation 07 (Earth).  
212 However, the Earth simulation is cooler because it has more snow & ice at high northerly  
213 latitudes and has a lower insolation.

214 The general effect of the different land/sea masks between Simulations 01–03 and  
215 04–06 and how they compare with modern Earth in Simulation 07 are seen in Supple-  
216 mentary Material Figures S1 and S2. In Figure S1 we plot the stream function which  
217 indicates the strength of the Hadley circulation. While the Amasia stream function is  
218 roughly the same as modern day Earth’s, the Aurica stream function is about an order  
219 of magnitude weaker. Surely this is due to the large super continent at low latitudes in  
220 the Aurica simulation that prevent moisture uptake at these lower latitudes.

221 On the other hand in Figure S2 we plot the Atmospheric, Oceanic and Total (At-  
222 mospheric + Ocean) meridional heat transport in units of petawatts. Simulations 01–  
223 03 (Aurica) and 07 (Earth) are decidedly similar, while that of Amasia appears to be  
224 generally stronger. The largest differences are the ocean transport in the middle figures  
225 where the low latitude landmass of Aurica prevents large meridional flows, whereas the  
226 lack of low-latitude landmasses in Simulations 04–06 (Amasia) allow for greater trans-  
227 port. Similar contrasts were seen in ancient Venus simulations at the inner edge of the  
228 habitable zone (Way et al., 2016) where a land-sea mask with more land at lower lat-  
229 itudes, versus modern Earth, generated distinct global mean surface temperatures.

230 We were not able to discern any marked differences in climate due to the day length  
231 being 30 minutes longer. This was examined by looking at the difference between Sim-  
232 ulation 07, which uses a modern Earth day length, and the same simulation (unpublished)  
233 using the same day length as Simulations 01–06. So, any differences between Simulations  
234 01–06 and Simulation 07 mentioned above are likely to due to differences in land-sea mask,  
235 insolation, and associated climate dynamics.

236 Work by Spiegel et al. (2008) uses a metric of “climatic habitability” that defines  
237 the amount of surface area of a planet that can host liquid water (e.g., surface temper-  
238 atures in the range  $0 < T < 100^{\circ}\text{C}$ ) at modern Earth atmospheric pressures. Again focus-  
239 ing on Simulation 02 and 05 we find that Simulation 02 has much less fractional hab-  
240 itability if we look at land and lakes – 58% – compared with Simulation 05 (99.8%). Sea  
241 surface temperatures are more balanced: Simulation 02 was at 73% and Simulation 05  
242 was at 71% habitability for the ocean. These numbers are all taken from averages of the  
243 last 10 years of each run.

## 244 4 Conclusions

245 The supercontinents of the future can provide us some guidance on how surface tem-  
246 peratures will increase or decrease depending on how the continents are distributed. But  
247 there are other factors to consider related to weathering rates and volcanic outgassing  
248 (e.g. Jellinek et al., 2019), not to mention the related role of atmospheric pressure (Gaillard  
249 & Scaillet, 2014).

250 As mentioned above, the small 30 minute decrease in rotation rate for Simulations  
251 01–06 as compared with modern Earth (Simulation 07) appears to play little or no role  
252 in the climate dynamics as there is no discernible difference in the strength or distribu-  
253 tion of the Hadley/Ferrell/Polar cells when comparing Simulation 05 and Simulation 07



254 (see Figure S2). There is a decrease in the strength of Simulation 02 compared to 07 (Fig-  
 255 ure S2), but this is likely due to the large low latitude supercontinent in Simulation 02.

256 While we discuss the future climate of Earth we do not touch on the future of life.  
 257 There are too many uncertainties for us to speculate, but recent work provides some guide-  
 258 lines (Mello & Friaça, 2019). The reduced tides during the supercontinent stage (Davies  
 259 et al., 2019) will lead to reduced vertical mixing rates, i.e. a reduced vertical diffusiv-  
 260 ity in the abyssal ocean (Munk, 1966; Wunsch & Ferrari, 2004). This may have impli-  
 261 cations for ocean ecosystems, and biodiversity. At the same time it appears that the for-  
 262 mation of Pangea had little effect on the global biodiversity of marine animals (Zaffos  
 263 & Peters, 2017) and Pangea was in a very weak tidal state (Green et al., 2017).

264 It would be interesting to compare the GCM derived climates for the superconti-  
 265 nent at low latitude in the Aurica runs with previous work on Pangea (e.g. Chandler et  
 266 al., 1992; Chandler, 1994; Fluteau et al., 2001; Gibbs et al., 2002; Roscher et al., 2011).  
 267 Unfortunately it is difficult to make a proper comparison for a number of reasons. First,  
 268 all of these previous works use either atmosphere only GCMs (i.e., no ocean) or shallow  
 269 mixed layer oceans with either prescribed horizontal heat transport or none at all. Sec-  
 270 ondly, unlike Aurica, Pangea spanned not only lower latitudes (like Aurica), but also high  
 271 southern latitudes where ice/snow forms easily (e.g. Chandler et al., 1992, see Figure 5).  
 272 Finally, there are different reconstructions for different time periods and not all are di-  
 273 rectly comparable to those we simulate herein. This makes a direct comparison with Pangea  
 274 complicated and we leave such an analysis for the future.

275 These new reconstructions may prove useful for exoplanetary studies where researchers  
 276 will have a larger library of topographies and land/sea masks to chose from when esti-  
 277 mating the probability of surface habitability on neighboring worlds.

## 278 Acknowledgments

279 Thanks goes to Jeffrey Jonas at The Goddard Institute for Space Studies for his help  
 280 with the map overlays in Figure 2. This work was supported by NASA’s Nexus for Ex-  
 281 oplanet System Science (NExSS). Resources supporting this work were provided by the  
 282 NASA High-End Computing (HEC) Program through the NASA Center for Climate Sim-  
 283 ulation (NCCS) at Goddard Space Flight Center. MJW acknowledges support from the  
 284 GSFC Sellers Exoplanet Environments Collaboration (SEEC), which is funded by the  
 285 NASA Planetary Science Division’s Internal Scientist Funding Model. HSD acknowledges  
 286 funding from FCT (ref. UID/GEO/50019/2019—Instituto Dom Luiz; FCT PhD grant  
 287 ref. PD/BD/135068/2017). JCD acknowledges an FCT Researcher contract, an exploratory  
 288 project grant ref. IF/00702/2015, and the FCT project UID/GEO/50019/2019-IDL. JAMG  
 289 acknowledges funding from NERC, grant NE/S009566/1 (MATCH). All GCM NetCDF  
 290 data used in this publication can be downloaded from the NCCS data portal:

291 [https://portal.nccs.nasa.gov/GISS\\_modelE/ROCKE-3D/publication-supplements/](https://portal.nccs.nasa.gov/GISS_modelE/ROCKE-3D/publication-supplements/)

## 292 References

- 293 Barker, P. F. (2001). Scotia sea regional tectonic evolution: implications for mantle  
 294 flow and palaeocirculation. *Earth-Science Reviews*, 55, 1-39.
- 295 Chandler, M. A. (1994, 01). Depiction of modern and Pangean deserts: Evaluation  
 296 of GCM hydrological diagnostics for paleoclimate studies. In *Pangea:  
 297 Paleoclimate, Tectonics, and Sedimentation During Accretion, Zenith, and  
 298 Breakup of a Supercontinent*. Geological Society of America. Retrieved from  
 299 <https://doi.org/10.1130/SPE288-p117> doi: 10.1130/SPE288-p117
- 300 Chandler, M. A., Rind, D., & Ruedy, R. (1992, 05). Pangaeon during  
 301 the Early Jurassic: GCM simulations and the sedimentary record of pa-  
 302 leoclimate. *GSA Bulletin*, 104(5), 543-559. Retrieved from <https://>



- 303 doi.org/10.1130/0016-7606(1992)104<0543:PCDTEJ>2.3.CO;2 doi:  
 304 10.1130/0016-7606(1992)104<0543:PCDTEJ>2.3.CO;2
- 305 Claire, M. W., Sheets, J., Cohen, M., Ribas, I., Meadows, V. S., & Catling, D. C.  
 306 (2012, September). The Evolution of Solar Flux from 0.1 nm to 160  $\mu\text{m}$ :  
 307 Quantitative Estimates for Planetary Studies. *Astrophysical Journal*, 757, 95.  
 308 doi: 10.1088/0004-637X/757/1/95
- 309 Collins, M., Knutti, R., Arblaster, J., Dufresne, J.-L., Fichet, T., Friedling-  
 310 stein, P., ... Wehner, M. (2013). Long-term Climate Change: Projections,  
 311 Commitments and Irreversibility. *Climate Change 2013: The Physical Sci-*  
 312 *ence Basis. Contribution of Working Group I to the Fifth Assessment Re-*  
 313 *port of the Intergovernmental Panel on Climate Change*, 1029–1136. doi:  
 314 10.1017/CBO9781107415324.024
- 315 Davies, H. S., Green, J. A. M., & Duarte, J. C. (2018). Back to the future: Test-  
 316 ing different scenarios for the next supercontinent gathering. *Global Planetary*  
 317 *Change*, 169, 133–144.
- 318 Davies, H. S., Green, J. A. M., & Duarte, J. C. (2019). Back to the future ii: Tidal  
 319 evolution of four supercontinent scenarios. *Earth System Dynamics*, submit-  
 320 ted.
- 321 DeConto, R. M., & Pollard, D. (2003). Rapid Cenozoic glaciation of Antarctica in-  
 322 duced by declining atmospheric CO<sub>2</sub>. *Nature*, 421, 245–249.
- 323 Duarte, J. C., Schellart, W. P., & Rosas, F. M. (2018). The future of Earth's  
 324 oceans: Consequences of subduction initiation in the Atlantic and implica-  
 325 tions for supercontinent formation. *Geological Magazine*, 155(1), 45–58. doi:  
 326 10.1017/S0016756816000716
- 327 Farnsworth, A., Lunt, D., O'Brien, C., Foster, G., Inglis, G., Markwick, P., ...  
 328 Robinson, S. (2019). Climate sensitivity on geological timescales controlled  
 329 by non-linear feedbacks and ocean circulation. *Geophysical Research Letters*,  
 330 2019GL083574.
- 331 Fluteau, F., Besse, J., Broutin, J., & Ramstein, G. (2001). The late permian cli-  
 332 mate. what can be inferred from climate modelling concerning pangea scenar-  
 333 ios and hercynian range altitude? *Palaeogeography, Palaeoclimatology, Palaeoe-*  
 334 *cology*, 167(1), 39 - 71. Retrieved from [http://www.sciencedirect.com/  
 335 science/article/pii/S0031018200002303](http://www.sciencedirect.com/science/article/pii/S0031018200002303) doi: [https://doi.org/10.1016/  
 336 S0031-0182\(00\)00230-3](https://doi.org/10.1016/S0031-0182(00)00230-3)
- 337 Gaillard, F., & Scaillet, B. (2014, Oct). A theoretical framework for volcanic de-  
 338 gassing chemistry in a comparative planetology perspective and implications  
 339 for planetary atmospheres. *Earth and Planetary Science Letters*, 403, 307-316.  
 340 doi: 10.1016/j.epsl.2014.07.009
- 341 Gibbs, M. T., Rees, P. M., Kutzbach, J. E., Ziegler, A. M., Behling, P. J., & Row-  
 342 ley, D. B. (2002). Simulations of permian climate and comparisons with  
 343 climate-sensitive sediments. *The Journal of Geology*, 110(1), 33-55. Retrieved  
 344 from <https://doi.org/10.1086/324204> doi: 10.1086/324204
- 345 Green, J. A. M., Huber, M., Waltham, D., Buzan, J., & Wells, M. (2017). Ex-  
 346 plicitly modelled deep-time tidal dissipation and its implication for lu-  
 347 nar history. *Earth and Planetary Science Letters*, 461, 46–53. doi:  
 348 10.1016/j.epsl.2016.12.038
- 349 Green, J. A. M., Molloy, J. L., Davies, H. S., & Duarte, J. C. (2018). Is there a tec-  
 350 tonically driven supertidal cycle? *Geophysical Research Letters*, 45, 3568–3576.  
 351 doi: 10.1002/2017GL076695
- 352 Huber, B. T., MacLeod, K. G., Watkins, D. K., & Coffin, M. F. (2018). The rise and  
 353 fall of the cretaceous hot greenhouse climate. *Global and Planetary Change*,  
 354 167, 1 - 23. doi: <https://doi.org/10.1016/j.gloplacha.2018.04.004>
- 355 Jellinek, M., Lenardic, A., & Pierrehumbert, R. (2019, 06). Ice, fire or fizzle: The  
 356 climate footprint of earth's supercontinental cycles. *Geochemistry, Geophysics,*  
 357 *Geosystems*, 10.

- 358 Krijgsman, W., Hilgen, F. J., Raffi, I., Sierro, F. J., & Wilson, D. S. (1999).  
 359 Chronology, causes and progression of the Messinian salinity crisis. *Nature*,  
 360 *400*(6745), 652–655.
- 361 MacDonald, G. J. F. (1964, 8). Tidal friction. *Reviews of Geophysics*, *2*(3), 467–  
 362 541. Retrieved from <https://doi.org/10.1029/RG002i003p00467> doi: 10  
 363 .1029/RG002i003p00467
- 364 Mello, F. d. S., & Friça, A. C. S. (2019). The end of life on earth is not the end  
 365 of the world: converging to an estimate of life span of the biosphere? *Internat-*  
 366 *ional Journal of Astrobiology*, 1-18. doi: 10.1017/S1473550419000120
- 367 Mitchell, R. N., Kilian, T. M., & Evans, D. A. D. (2012). Supercontinent cycles  
 368 and the calculation of absolute palaeolongitude in deep time. *Nature*, *482*,  
 369 208–211.
- 370 Montes, C., Cardona, A., Jaramillo, C., Pardo, A., Silva, J. C., Valencia, V., ...  
 371 Niño, H. (2015). Middle Miocene closure of the Central American Seaway.  
 372 *Science*, *348*, 226–229.
- 373 Munk, W. H. (1966). Abyssal recipes. *Deep-Sea Research and Oceanographic Ab-*  
 374 *stracts*, *13*(4), 707–730. doi: 10.1016/0011-7471(66)90602-4
- 375 Parrish, J. (1993, 03). Climate of the supercontinent pangea. *Journal of Geology*,  
 376 *101*, 215-233. doi: 10.1086/648217
- 377 Pastor-Galán, D., Nance, R. D., Murphy, J. B., & Spencer, C. J. (2019). Su-  
 378 percontinents: myths, mysteries, and milestones. *Geological Society,*  
 379 *London, Special Publications*, *470*(1), 39–64. Retrieved from [https://](https://sp.lyellcollection.org/content/470/1/39)  
 380 [sp.lyellcollection.org/content/470/1/39](https://sp.lyellcollection.org/content/470/1/39) doi: 10.1144/SP470.16
- 381 Pierrehumbert, R. T., Abbot, D. S., Voigt, A., & Koll, D. (2011). Climate of the  
 382 neoproterozoic. *Annual Reviews of Earth and Planetary Sciences*, 417-460.
- 383 Roscher, M., Stordal, F., & Svensen, H. (2011). The effect of global warming and  
 384 global cooling on the distribution of the latest permian climate zones. *Palaeo-*  
 385 *geography, Palaeoclimatology, Palaeoecology*, *309*(3), 186 - 200. Retrieved from  
 386 <http://www.sciencedirect.com/science/article/pii/S0031018211002987>  
 387 doi: <https://doi.org/10.1016/j.palaeo.2011.05.042>
- 388 Schmittner, A., Silva, T. A. M., Fraedrich, K., Kirk, E., & Lunkeit, F. (2011). Ef-  
 389 fects of Mountains and Ice Sheets on Global Ocean Circulation. *Journal of Cli-*  
 390 *mate*, *24*, 2814–2829.
- 391 Spiegel, D. S., Menou, K., & Scharf, C. A. (2008, Jul). Habitable Climates. *Astro-*  
 392 *physical Journal*, *681*(2), 1609-1623. doi: 10.1086/588089
- 393 Tada, R., Zheng, H., & Clift, P. D. (2016). Evolution and variability of the Asian  
 394 monsoon and its potential linkage with uplift of the Himalaya and Tibetan  
 395 Plateau. *Progress in Earth and Planetary Science*, *3*, 4.
- 396 Way, M. J., Aleinov, I., Amundsen, D. S., Chandler, M. A., Clune, T. L., Del  
 397 Genio, A. D., ... Tsigaridis, K. (2017, July). Resolving Orbital and Cli-  
 398 mate Keys of Earth and Extraterrestrial Environments with Dynamics  
 399 (ROCKE-3D) 1.0: A General Circulation Model for Simulating the Climates  
 400 of Rocky Planets. *Astrophysical Journal Supplement Series*, *231*, 12. doi:  
 401 10.3847/1538-4365/aa7a06
- 402 Way, M. J., Del Genio, A. D., Aleinov, I., Clune, T. L., Robinson, T. D., Kelly, M.,  
 403 & Kiang, N. Y. (2018). Climates of warm earth-like planets. i. 3d model  
 404 simulations. *The Astrophysical Journal Supplement Series*, *239*(2).
- 405 Way, M. J., Genio, A. D. D., Kiang, N. Y., Sohl, L. E., Grinspoon, D. H., Aleinov,  
 406 I., ... Al, W. A. Y. E. T. (2016). Was Venus the first habitable world of our  
 407 solar system? *Geophysical Research Letters*, *43*, 8376-8383.
- 408 Wunsch, C., & Ferrari, R. (2004). Vertical mixing, energy, and the general circula-  
 409 tion of the oceans. *Annual Review of Fluid Mechanics*, *36*(1), 281–314.
- 410 Yang, J., Boué, G., Fabrycky, D. C., & Abbot, D. S. (2014). Strong dependence of  
 411 the inner edge of the habitable zone on planetary rotation rate. *Astrophysical*  
 412 *Journal Letters*, *787*(1). doi: 10.1088/2041-8205/787/1/L2

- 413 Yoshida, M. (2016, 09). Formation of a future supercontinent through plate mo-  
 414 tion-driven flow coupled with mantle downwelling flow. *Geology*, *44*(9), 755-  
 415 758. Retrieved from <https://doi.org/10.1130/G38025.1> doi: 10.1130/  
 416 G38025.1
- 417 Yoshida, M., & Santosh, M. (2018). Voyage of the indian subcontinent since pangea  
 418 breakup and driving force of supercontinent cycles: Insights on dynamics from  
 419 numerical modeling. *Geoscience Frontiers*, *9*(5), 1279 - 1292. Retrieved from  
 420 <http://www.sciencedirect.com/science/article/pii/S1674987117301536>  
 421 (SPECIAL ISSUE: Frontiers in geoscience:A tribute to Prof. Xuanxue Mo)  
 422 doi: <https://doi.org/10.1016/j.gsf.2017.09.001>
- 423 Zaffos, S., A. Finneganb, & Peters, S. E. (2017). Plate tectonic regulation of  
 424 global marine animal diversity. *PNAS*, *114*(22), 5653–5658. Retrieved from  
 425 <https://www.pnas.org/content/114/22/5653> doi: [https://doi.org/10.1073/](https://doi.org/10.1073/pnas.1702297114)  
 426 [pnas.1702297114](https://doi.org/10.1073/pnas.1702297114)

**fig2d.png.**

## Simulation 02: Snow and ice coverage Jun/Jul/Aug

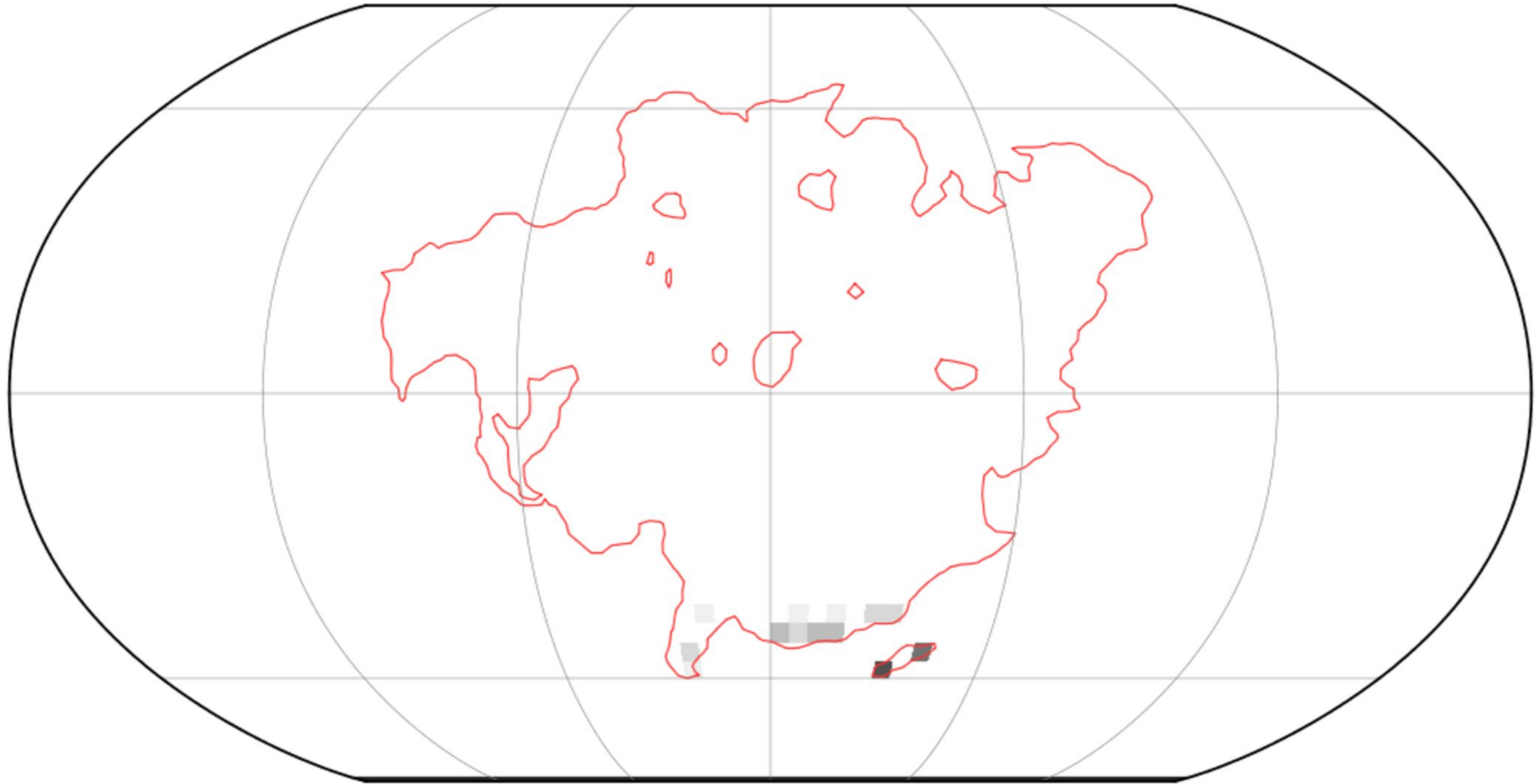


**fig2e.png.**



## Simulation 05: Snow and ice coverage Jun/Jul/Aug

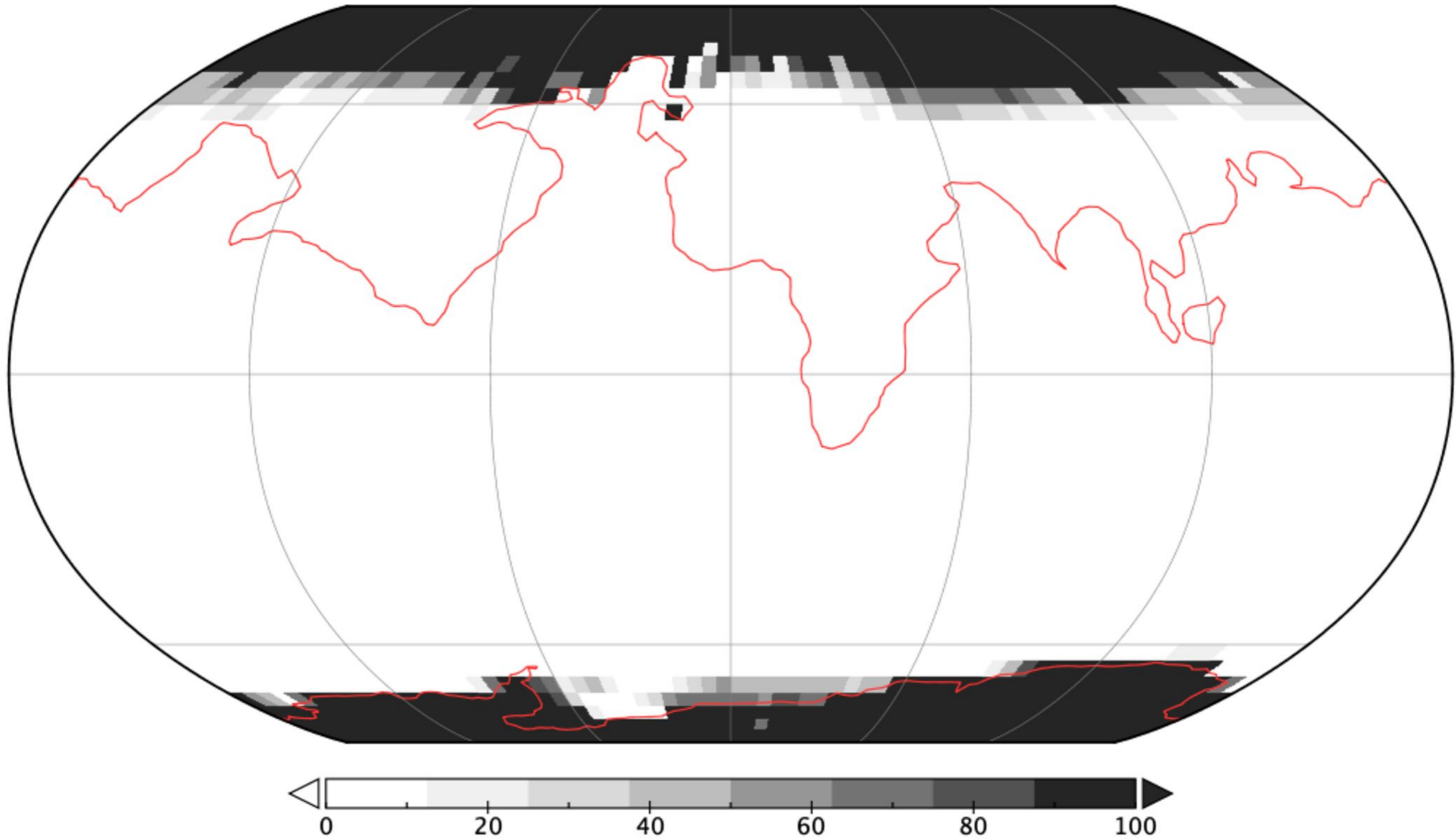


**fig2f.png.**

## Simulation 07: Snow and ice coverage Jun/Jul/Aug

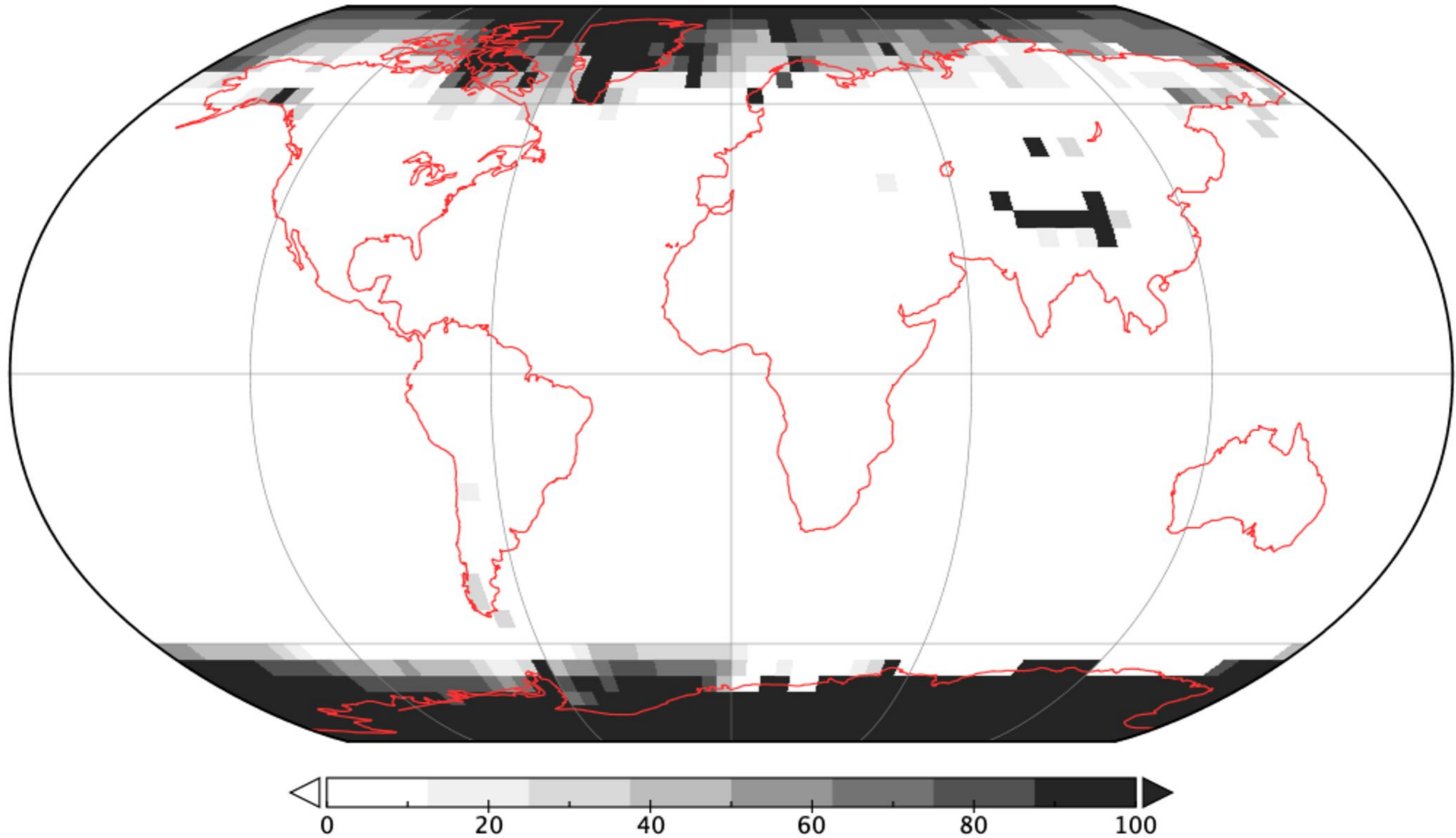


**fig1d.png.**

## Simulation 04: Amasia\_Rand\_CTRL

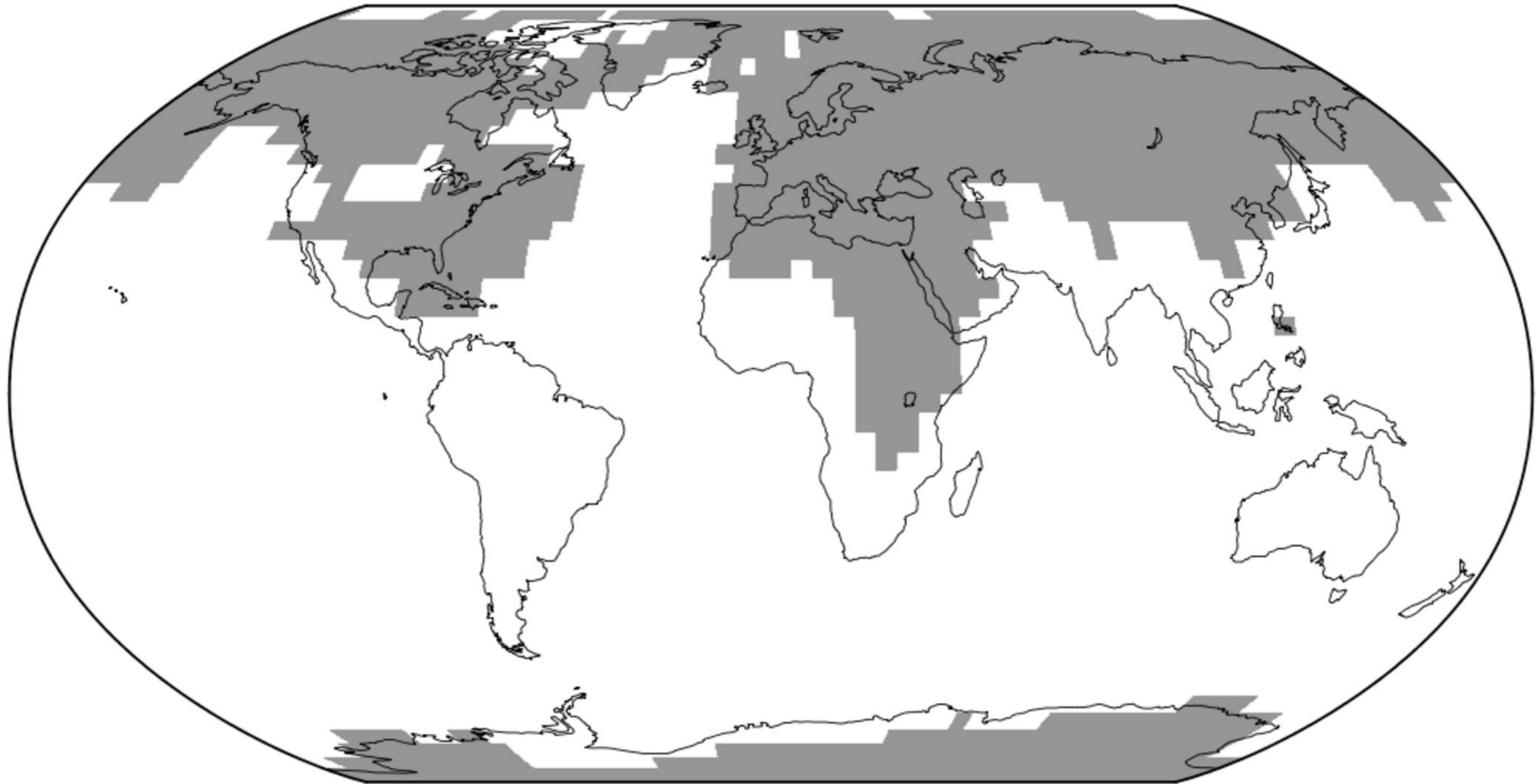


**fig2b.png.**



## Simulation 05: Snow and ice coverage Dec/Jan/Feb

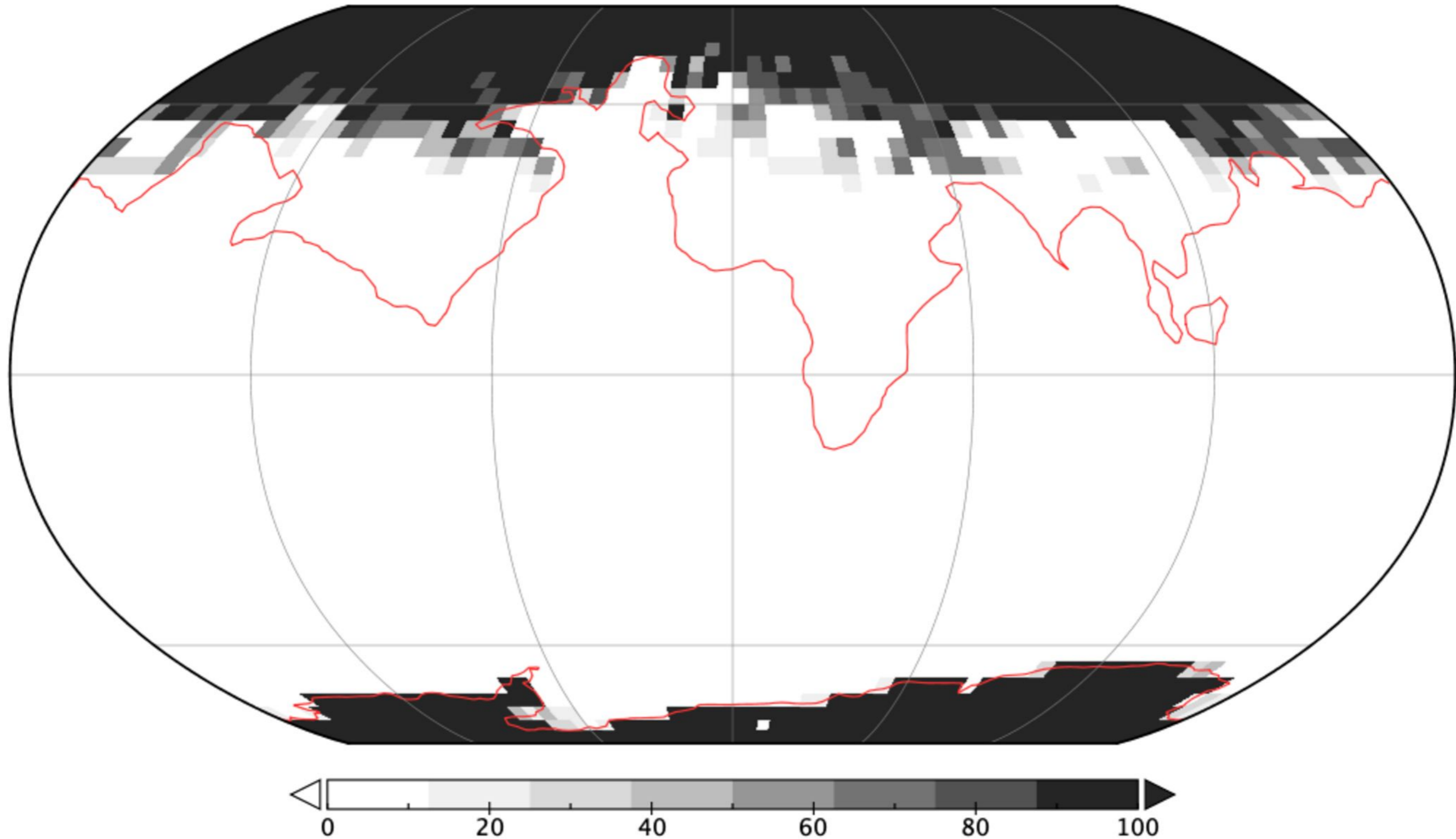
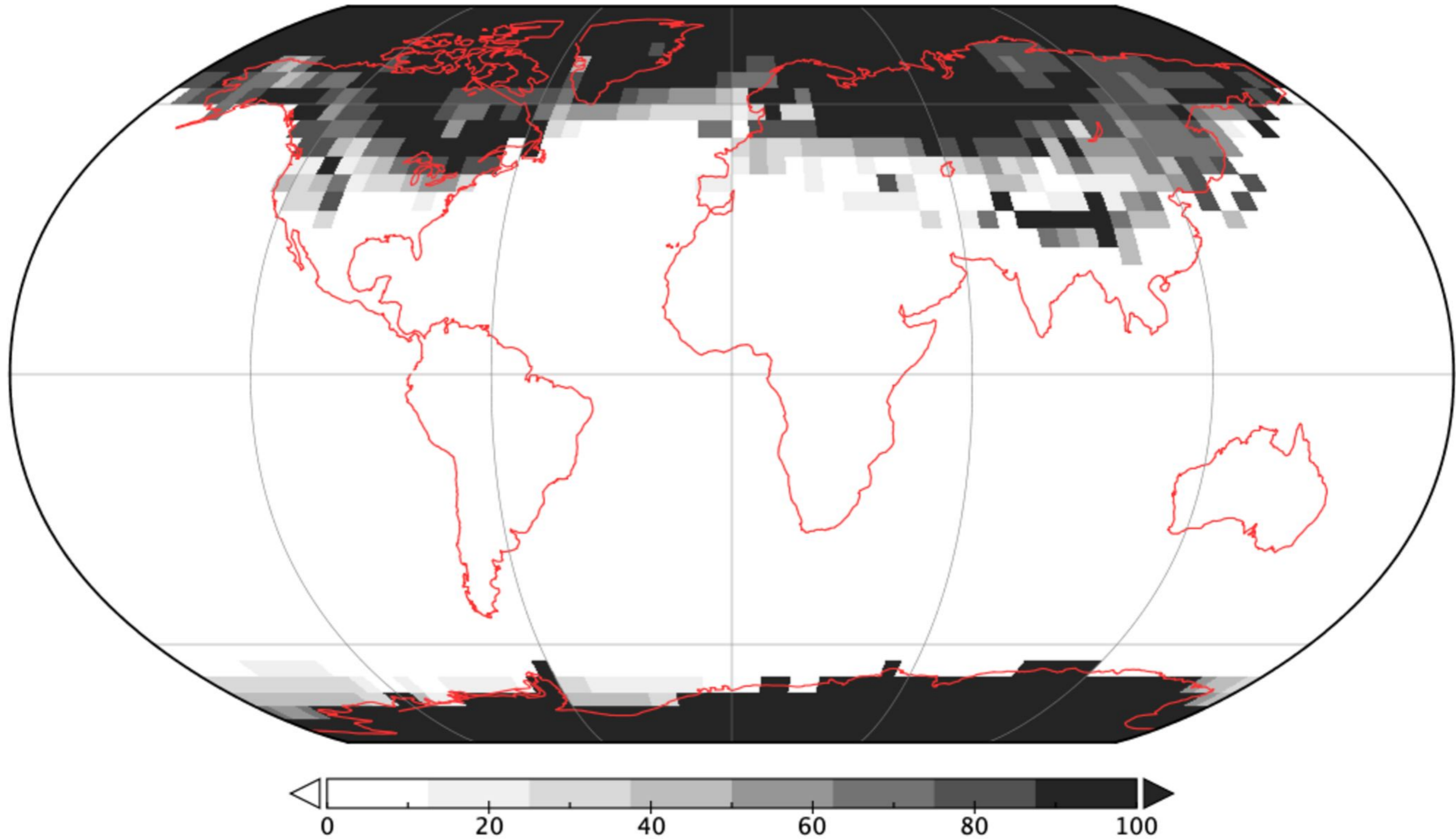


**fig2c.png.**

## Simulation 07: Snow and ice coverage Dec/Jan/Feb



**figS2c.png.**

# Simulation 07: Stream Function (kg/s)

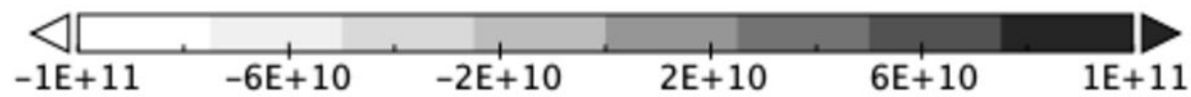
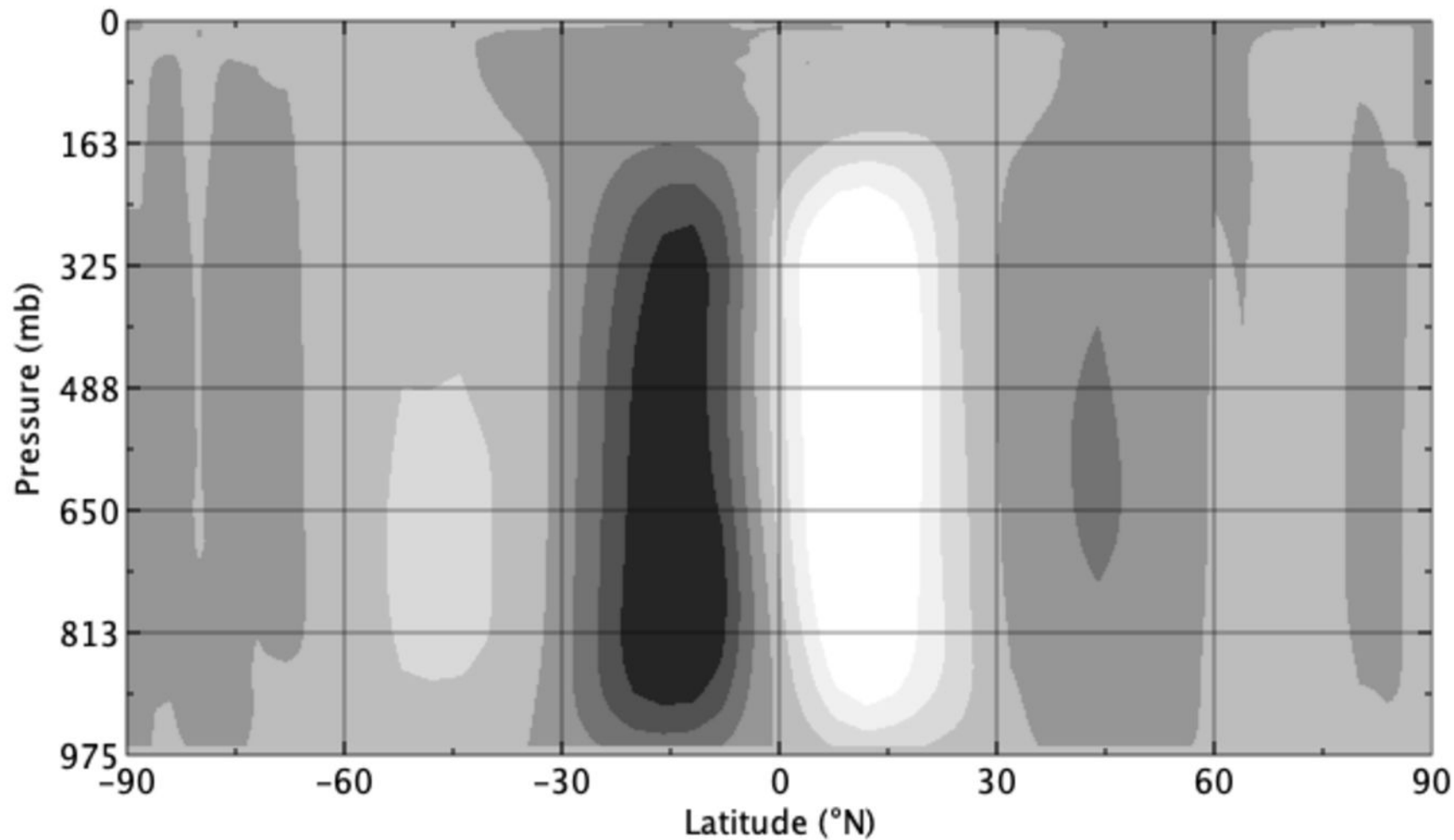
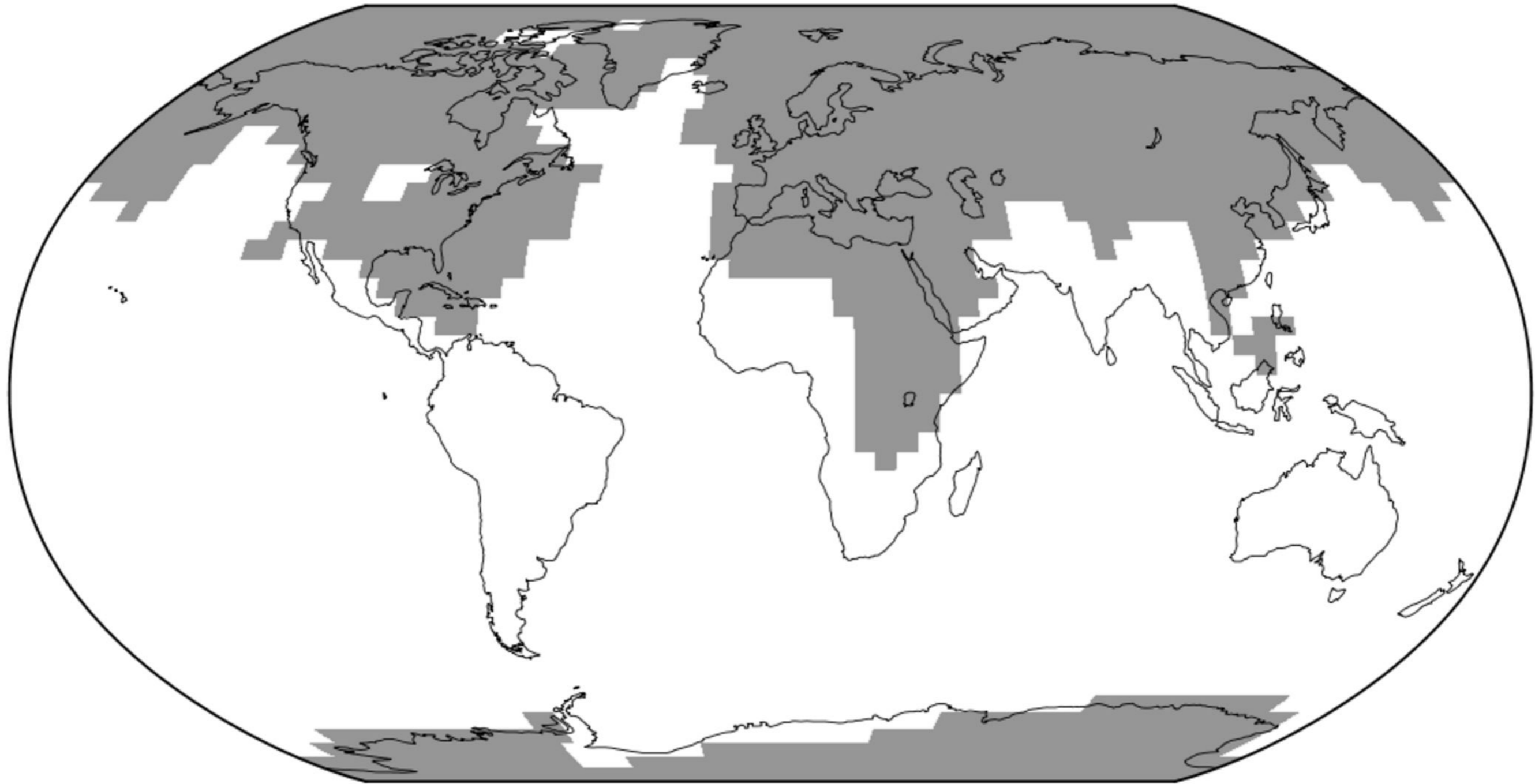


**fig1e.png.**



## Simulation 05: Amasia\_Rand\_PD



**figS2a.png.**

## Simulation 02: Stream Function (kg/s)

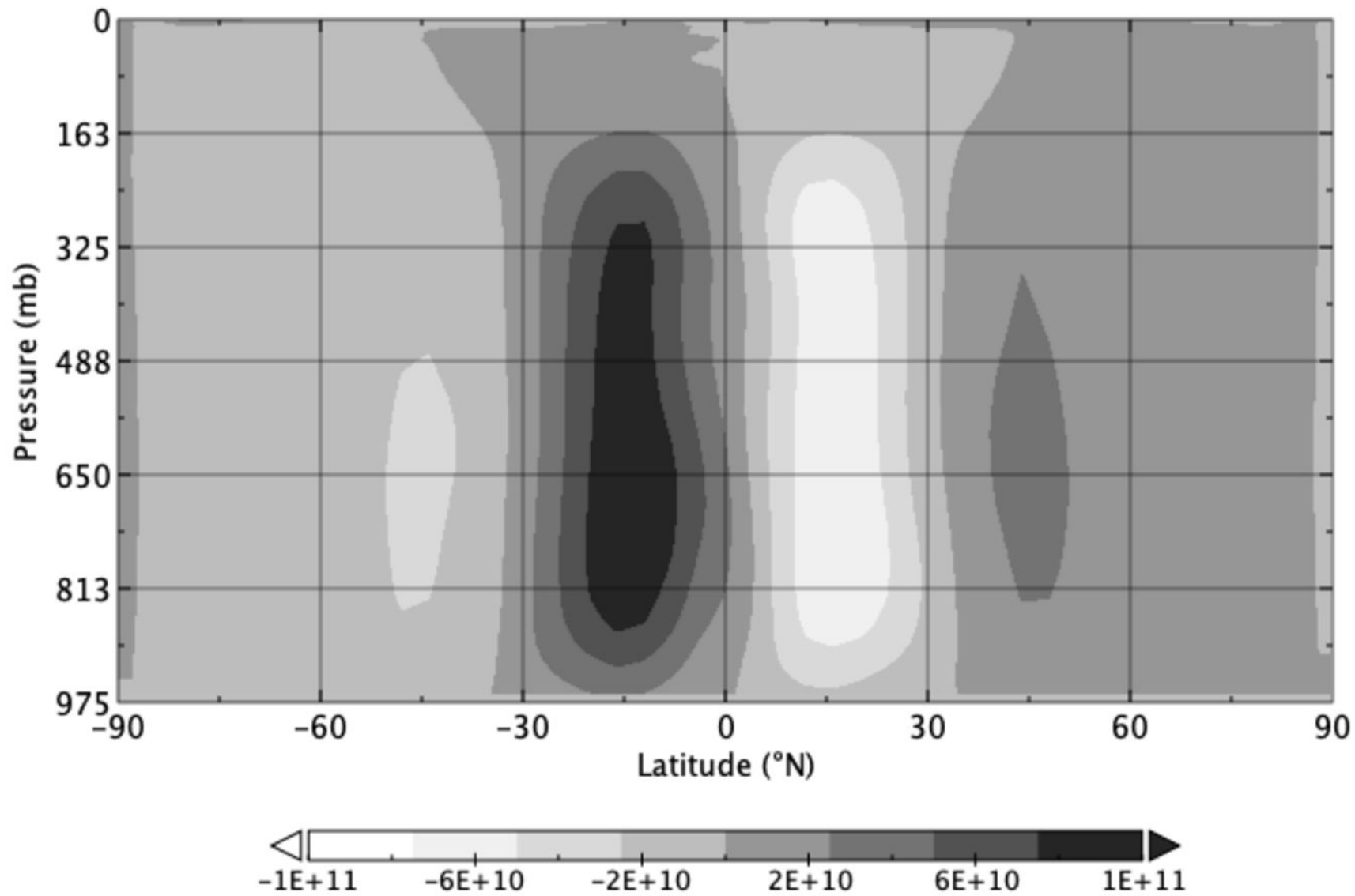


**fig1c.png.**

## Simulation 03: Aurica\_250f

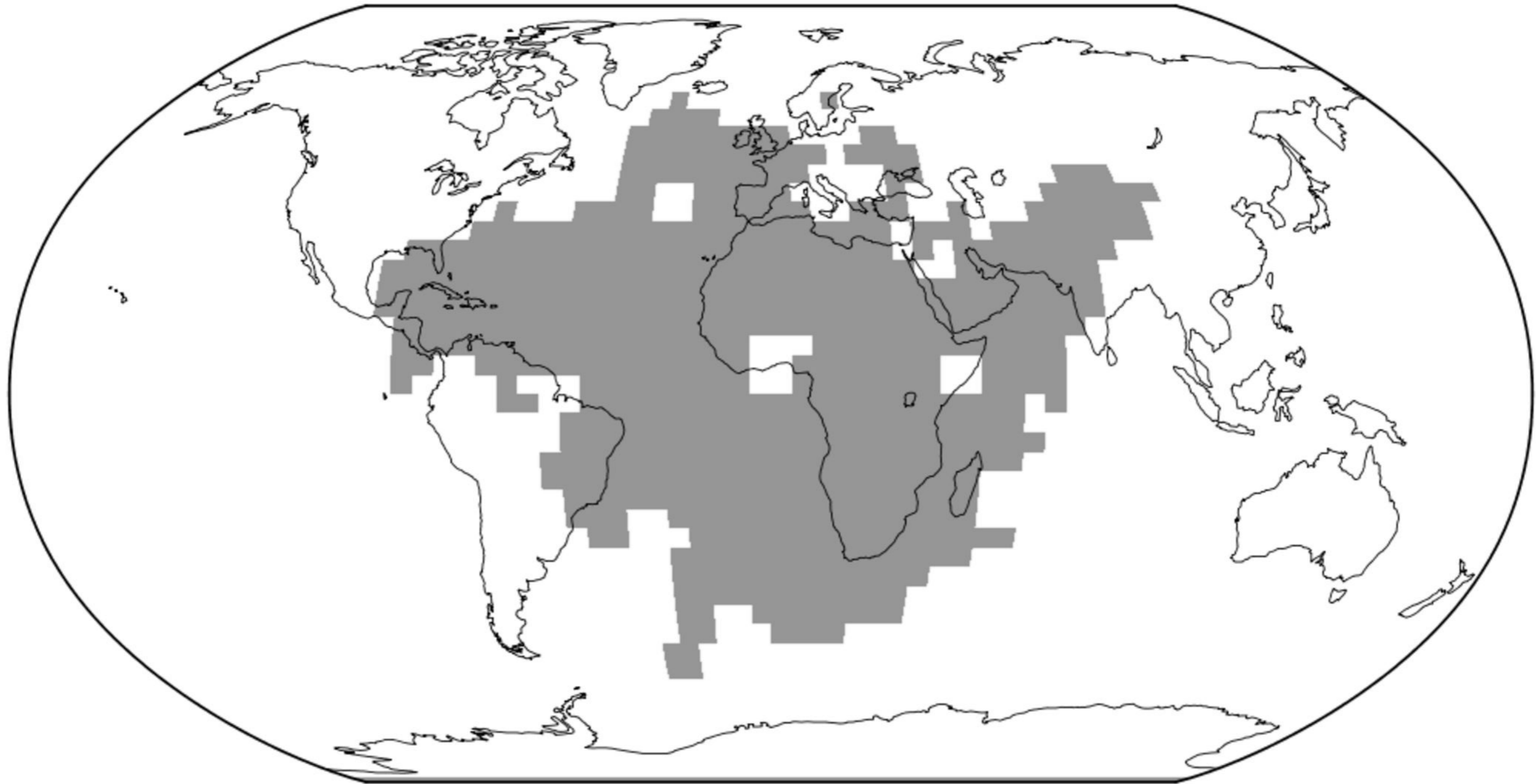


**fig1f.png.**

## Simulation 06: Amasia\_200f

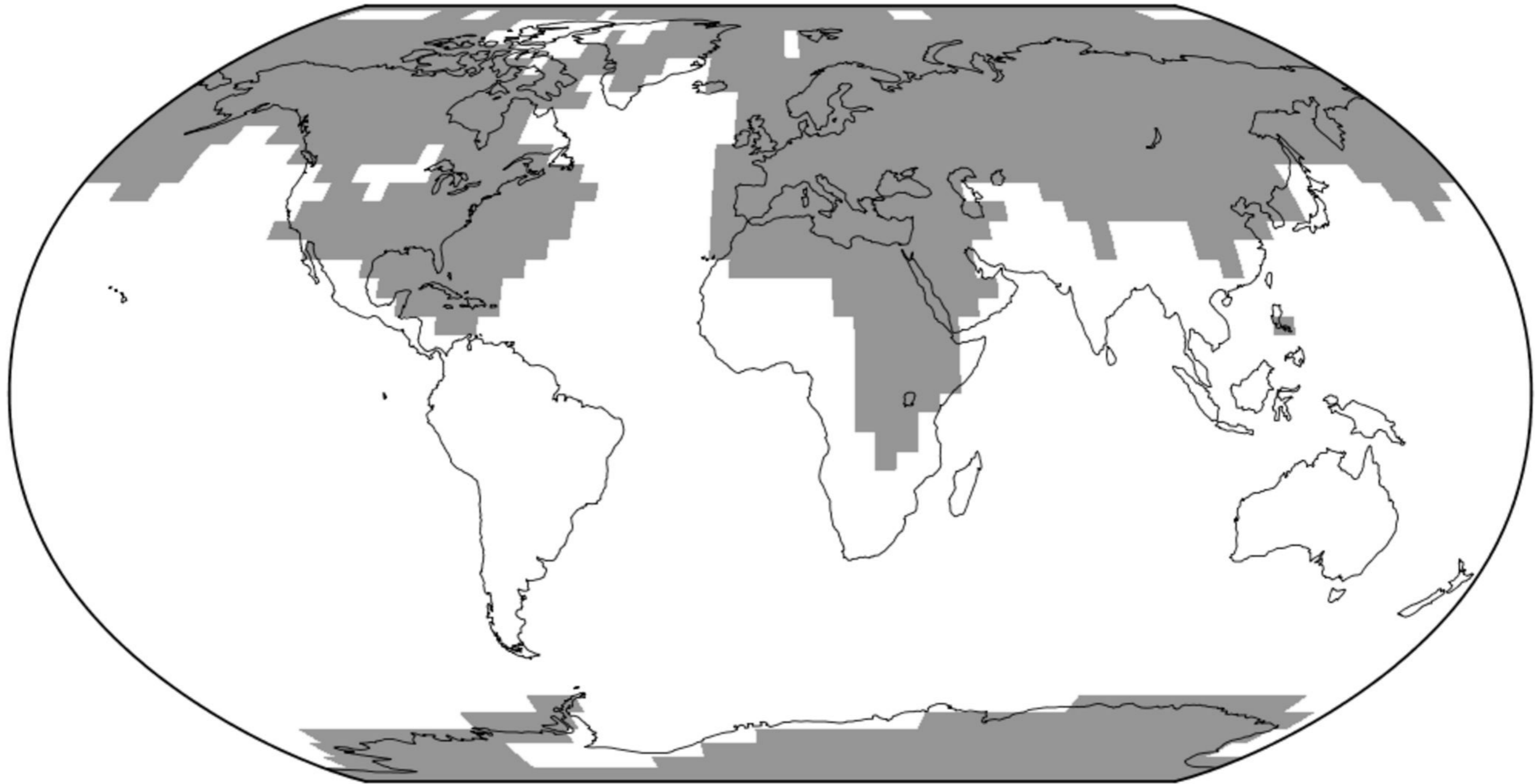
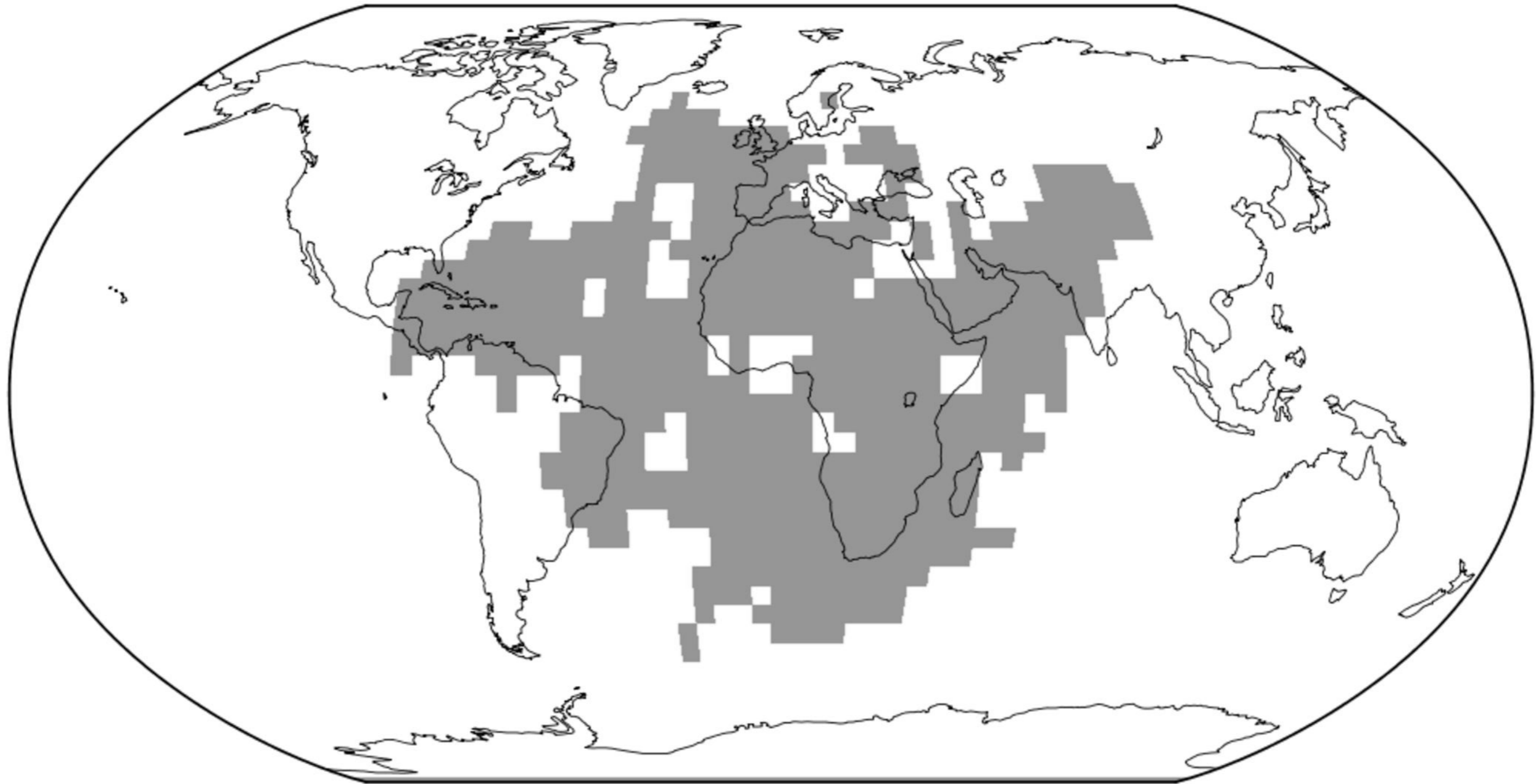


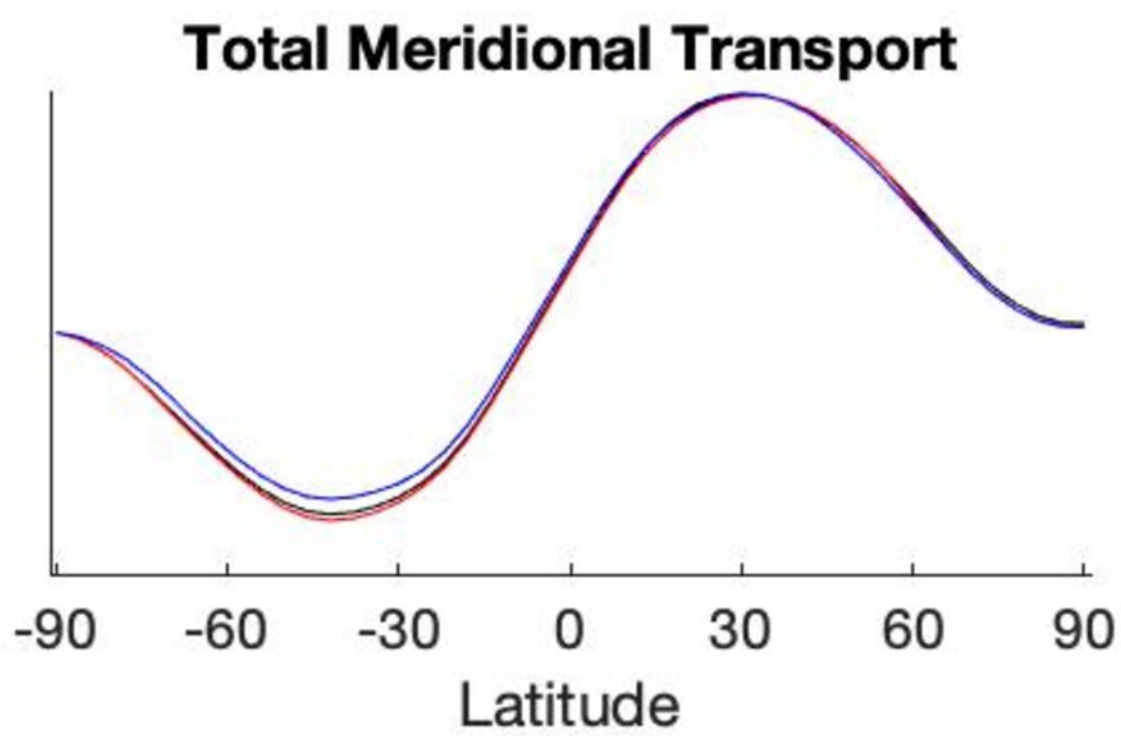
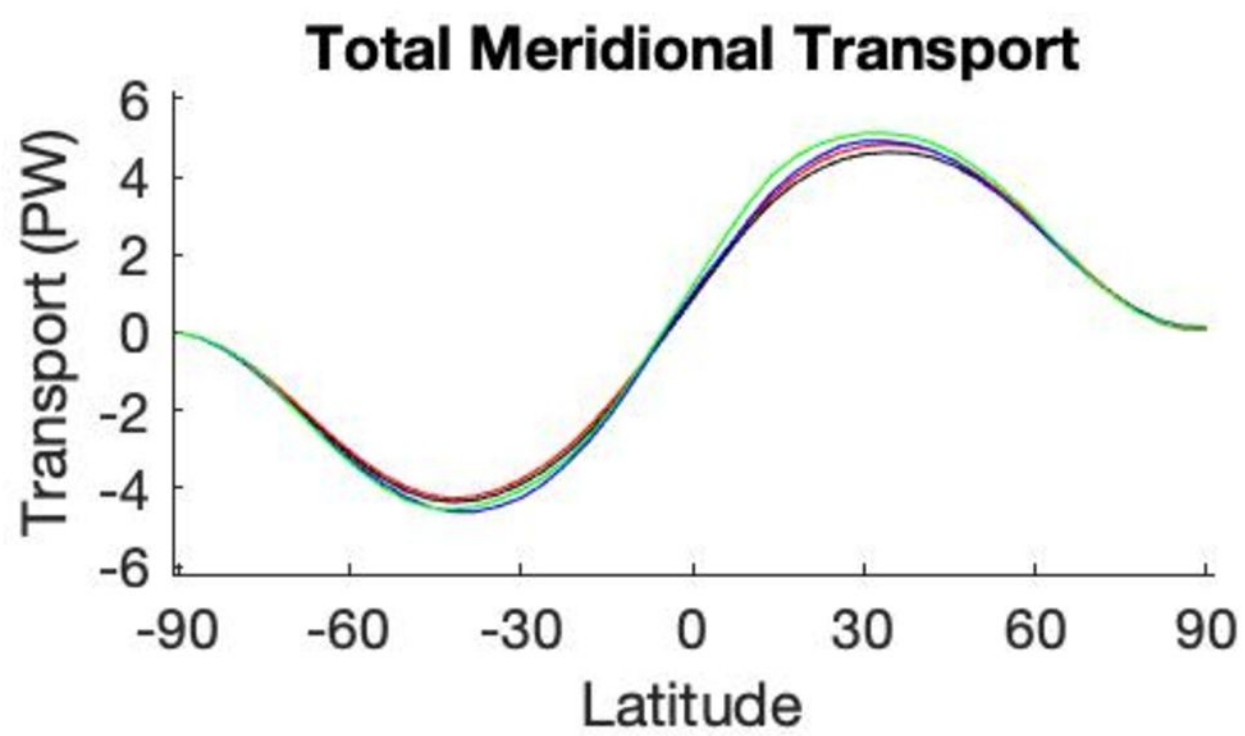
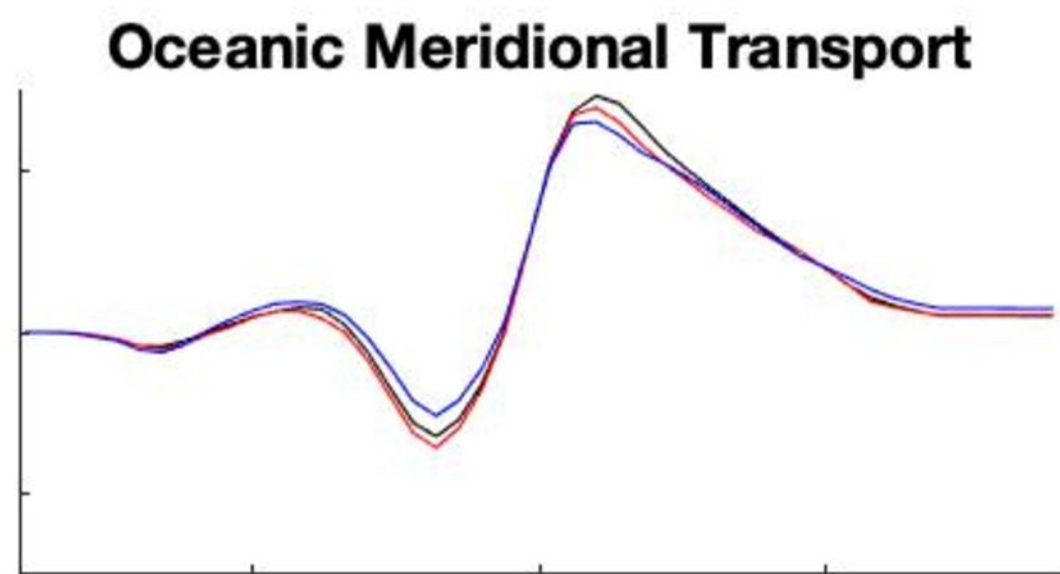
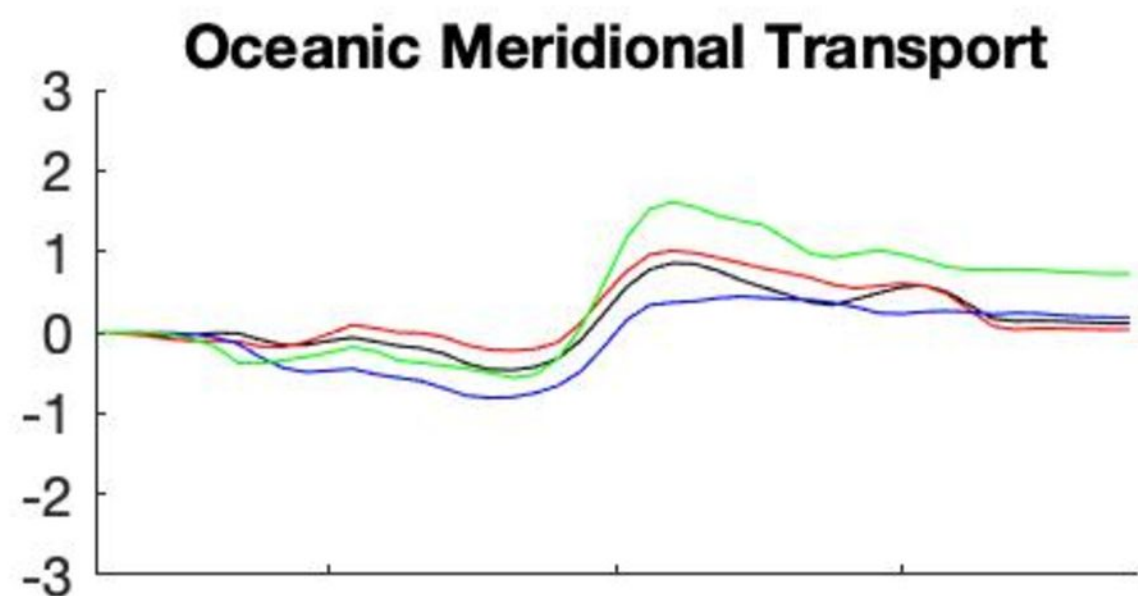
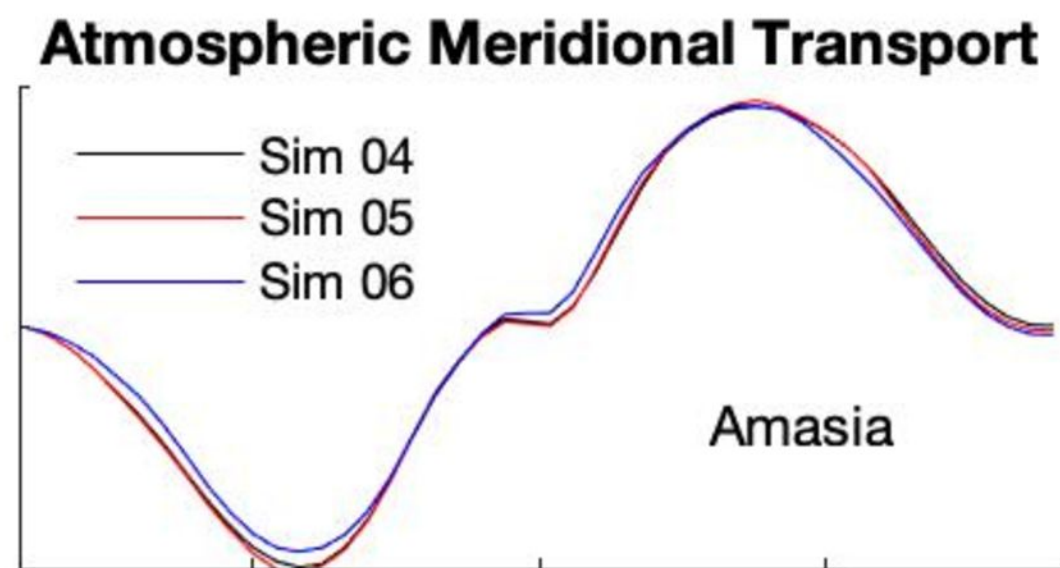
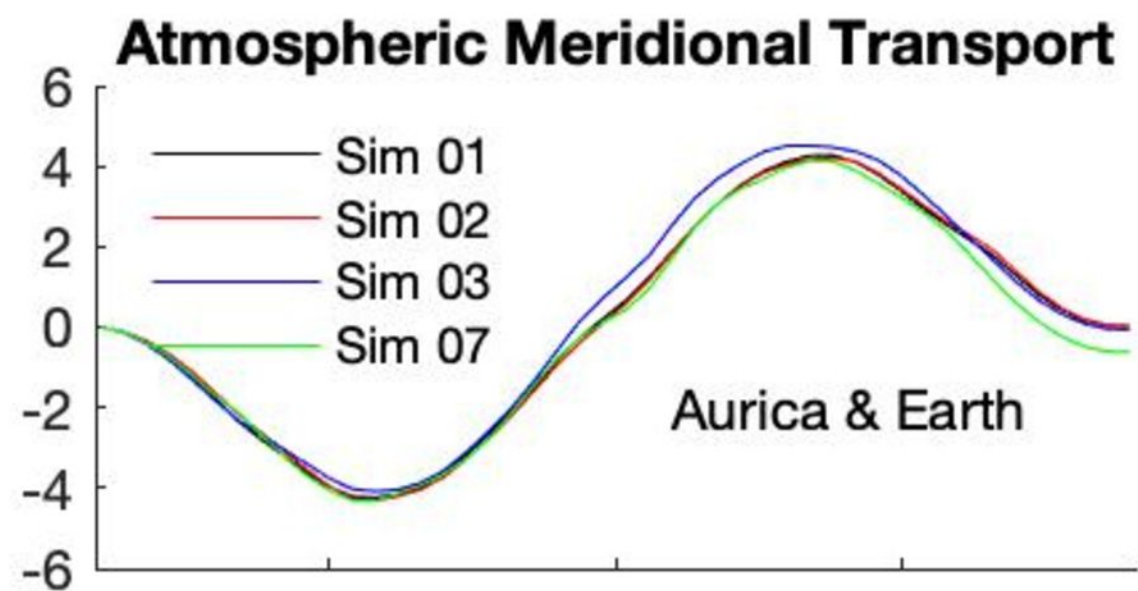
**Figure 1a.**



## Simulation 01: Aurica\_Rand\_CTRL



**figS1.png.**



**figS2b.png.**

# Simulation 05: Stream Function (kg/s)

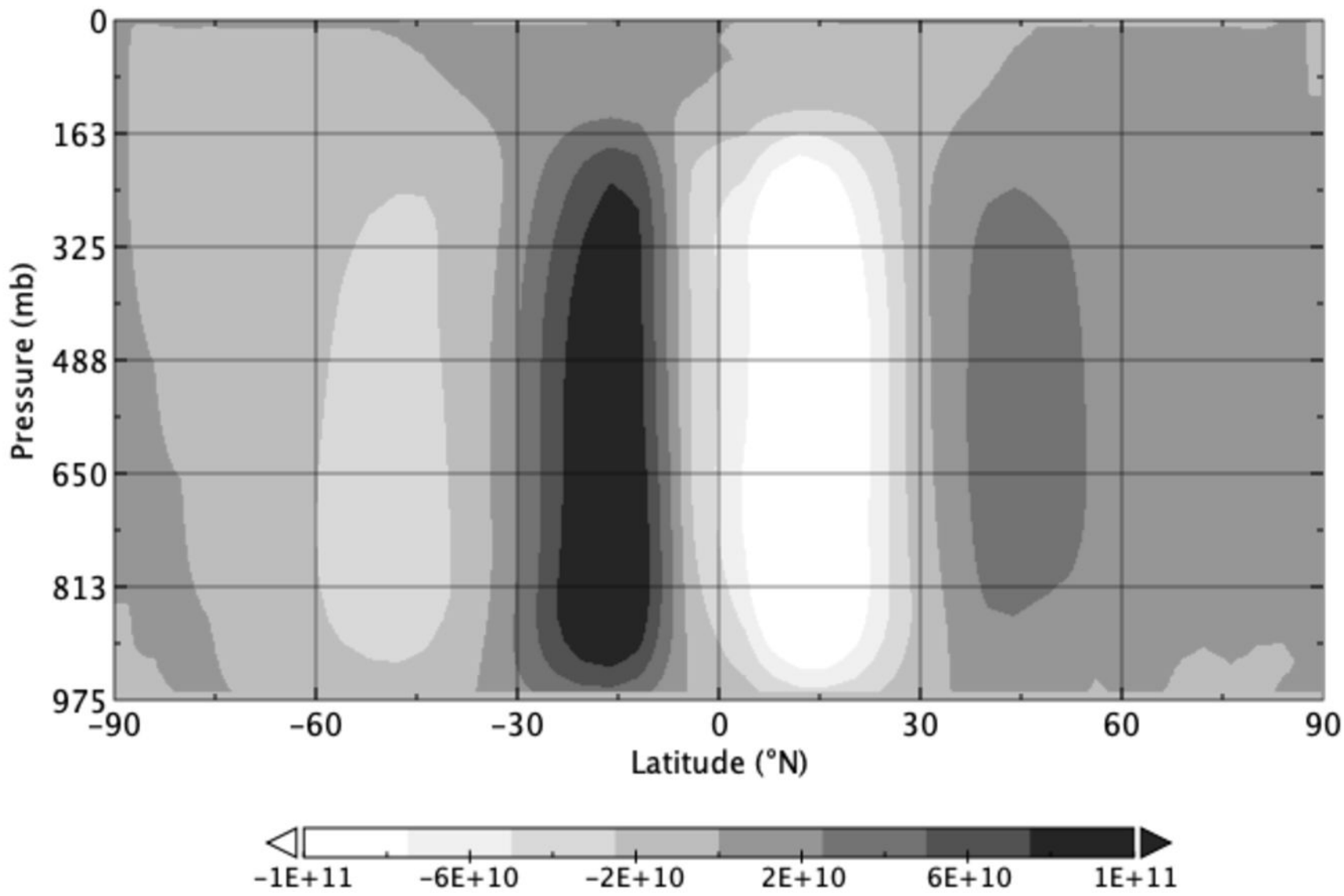


**fig2a.png.**

## Simulation 02: Snow and ice coverage Dec/Jan/Feb

